X. Research and Advanced Concepts

PROPULSION DIVISION

A. Hollow Cathode Operation in the SE-20C Thruster, *T. D. Masek and E. V. Pawlik*

1. Introduction

Operation of the SE-20C mercury ion thruster using an oxide cathode has been reported previously (Refs. 1 and 2). Interest in the hollow cathode, as discussed in SPS 37-48, Vol. III, pp. 119–125 and SPS 37-49, Vol. III, pp. 207–211, has resulted in adapting this cathode to the SE-20C. This article describes initial test results using an adjustable cathode pole piece and baffle assembly. The objectives of this work were the evaluation of the effect of

(1) The pole piece side slot and baffle open area on discharge losses.

(2) Introducing all the propellant flow through the cathode.

(3) Total flowrate on discharge losses.

2. Experimental Setup

The hollow cathode thruster was one of four thrusters mounted in a basic test array (Refs. 1 and 2). Except for the use of the SE-20C thruster and a pole piece assembly to be described later, the setup was similar to that reported in Ref. 1. A new cathode with a tip diameter of 0.42 cm, a tip thickness of 0.10 cm, and an orifice diameter of 0.05 cm was used.

The cathode pole piece and baffle assembly is shown in Fig. 1. The pole piece used in oxide cathode thruster designs forms the basic structure. The side of the pole piece was slotted in eight places (2.54 cm long, including circular ends, and 1.59 cm wide). A similarly slotted sleeve was fitted inside. Rotation of the sleeve relative to the pole piece varied the slot area from 0 to 28 cm^2. The baffle was constructed from two disks mounted on the same axis, each having four 1.59-cm-diameter holes. Rotation of the outer disk relative to the other disk fixed to the pole piece varied the baffle area from 0 to 7.9 cm^2. As shown in Fig. 1, both the sleeve and baffle were adjusted using gear sections. Shafts through the thruster backplate allowed these adjustments to be made from outside the vacuum chamber while the thruster was operating.

3. Test Results

Operation at a single cathode flowrate (3.35 g/h) was sufficient to obtain the data of interest. Using this

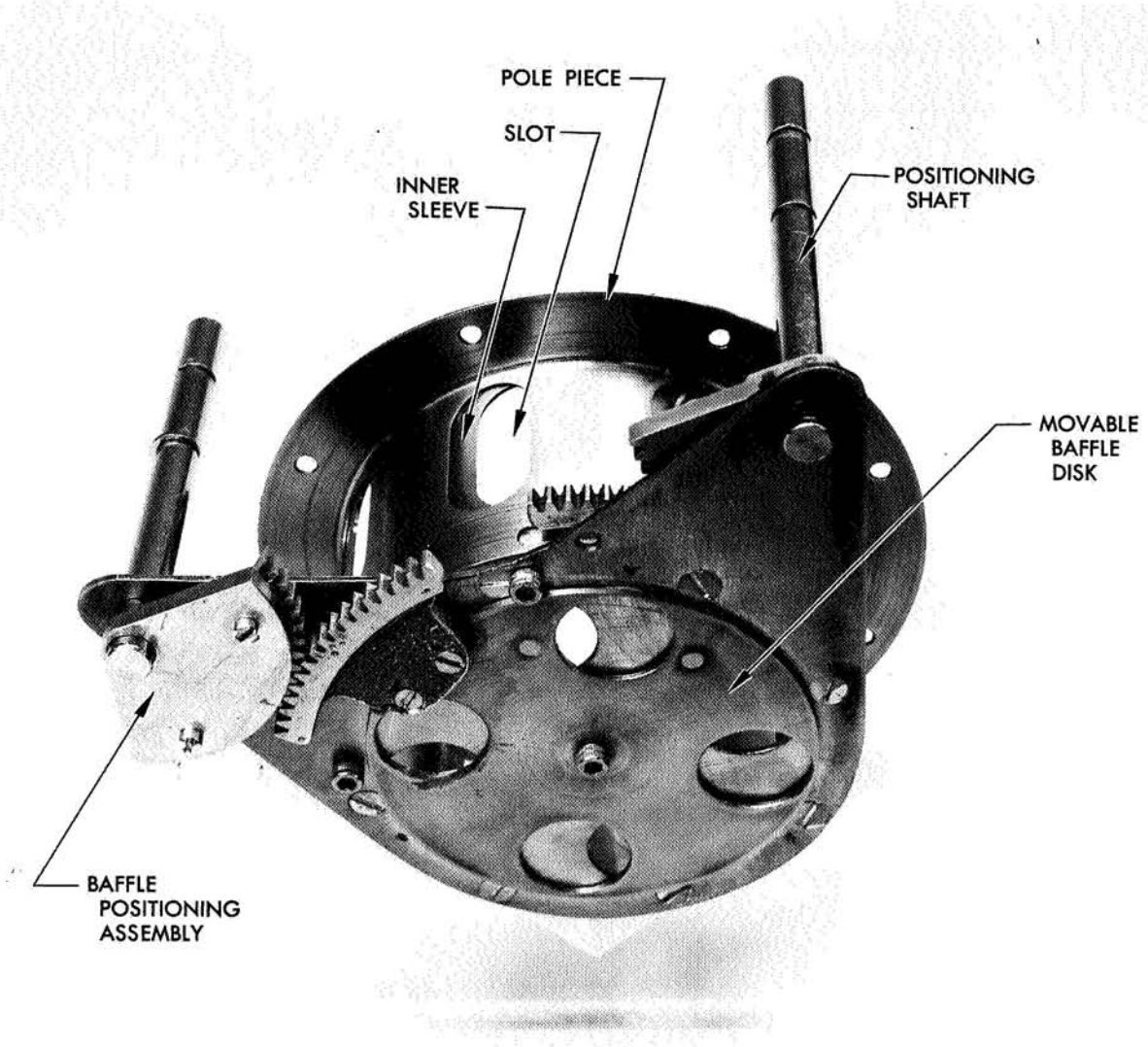

Fig. 1. Variable-area cathode baffle

cathode flow, the thruster was tested with other main flowrates. Because of limited test time, the pole piece slot was adjusted for minimum discharge losses at the beginning (only cathode flow) and remained fixed. This slot area was 9.5 cm².

Data showing the effect of baffle open area on discharge losses and utilization efficiency are shown in Fig. 2 for two flowrate conditions. The data show the best trade-off of discharge losses against utilization occurs at about 1.5 cm². Smaller areas increase the discharge losses with little or no change in utilization. This condition is similar for cathode flow alone and with main flow. Previous hollow cathode tests (SPS 37-48 and 37-49, Vol. III) with the SE-20B thruster, without pole piece slots, showed a baffle open area of 2.5 cm² was near optimum.

The effect of introducing all of the propellant through the cathode is also illustrated in Fig. 2. With only cathode flow, the discharge losses were approximately 760 eV/ion. With the addition of main flow, the losses were reduced 300 eV/ion. This result is consistent with physical reasoning and previous results. With only cathode flow, neutrals must be ionized within or near the pole piece. If not ionized in this region, the neutral flux is collimated by the pole piece baffle and can escape without a collision. Similar tests (Ref. 1) also indicated a fraction of

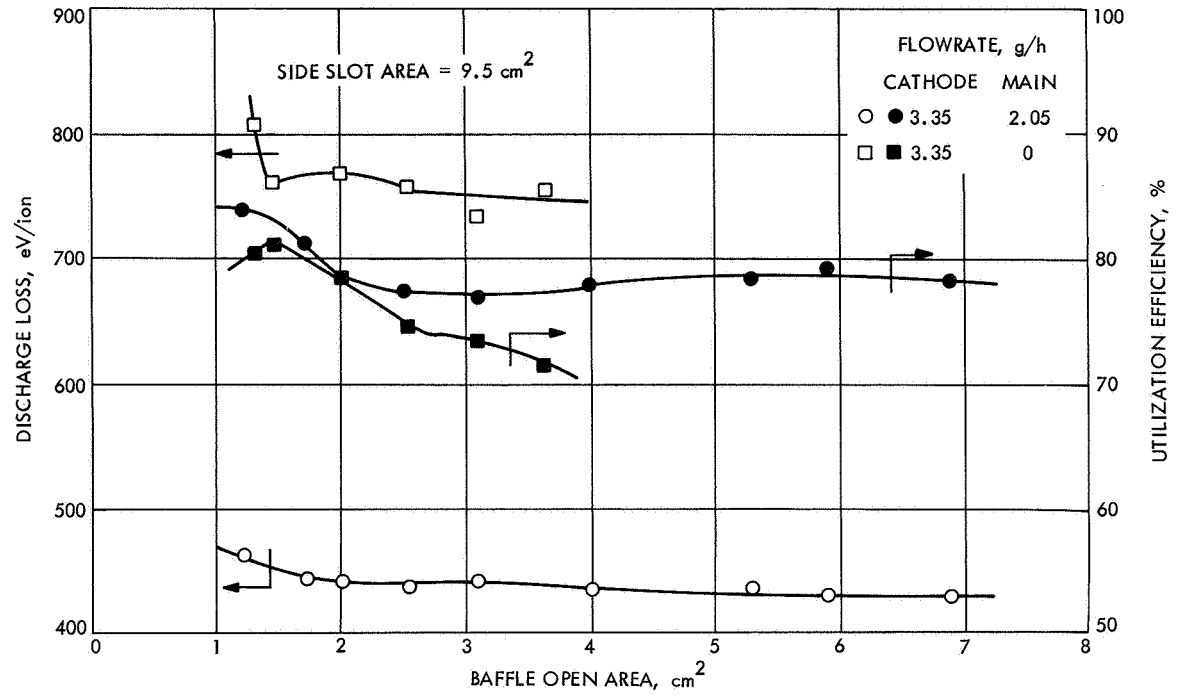

Fig. 2. Discharge loss and utilization efficiency as a function of baffle open area

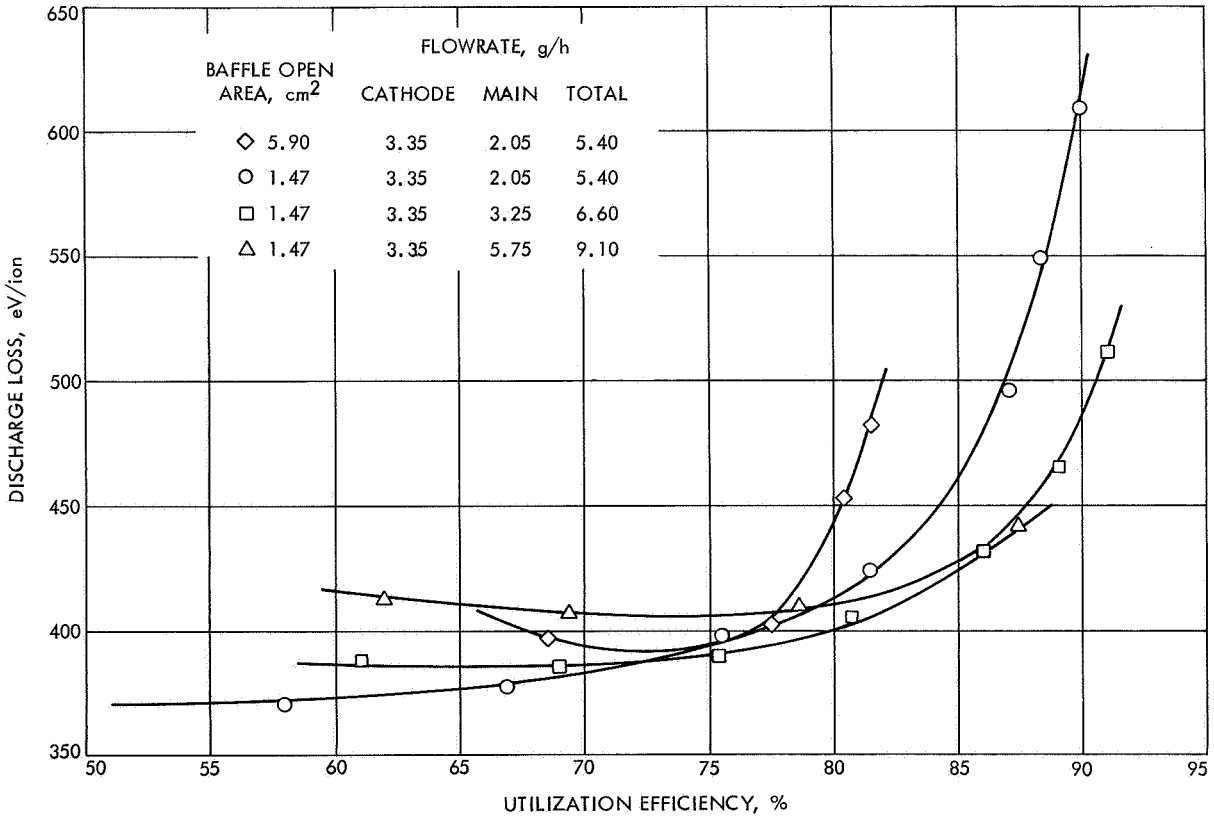

Fig. 3. Discharge loss variation for different baffle open areas and different total flowrates

the neutrals is lost directly when fed in from the rear. Raising the ionization fraction in the pole piece to prevent the loss of neutrals forces both the wall losses and basic ion production cost up. The addition of main flow makes the cathode flow relatively less important. The cathode density can then be reduced, decreasing cathode wall losses and ion production costs, and allowing more "primary" electrons to reach the main discharge chamber to ionize the main flow. This is a more efficient mode because the "reverse feed" main flow does not allow neutrals to escape without a collision.

The influence of main flow is illustrated further in Fig. 3. These data show a number of interesting effects. First, the effect of pole piece open area on the ability to obtain high utilization is shown. For the same total flowrate of 5.40 g/h, the curves are shifted by about 5% in utilization with different baffle open areas (1.47 and 5.90 cm^2). The more open condition apparently allows a higher fraction of neutrals to escape directly. Second, with the same baffle open area (1.47 cm^2), the data show that minimum discharge losses occur with a flowrate of about 6–7 g/h. This is also consistent with other results. When the cathode flow is as small as in Ref. 2, the curves shift consistently upward with increased flow. However, this "normal" trend is offset by the improvement provided by increasing the fraction of main flow. Note that the curves continue to shift toward higher utilization as the main flow fraction increases.

4. Conclusions

The results indicate that introducing all or a large fraction of the propellant through the cathode may limit utilization and increase discharge losses. Other configurations might avoid this difficulty. A good pole piece configuration was shown to be established rapidly (in one test) with the assembly used. Additional tests should be performed with the cathode in other positions and with other cathode flowrates. The change of discharge loss characteristics with flowrate supports physical arguments in describing discharge operation.

References

1. Masek, T. D., *Experimental Studies With a Mercury Bombardment Thrustor System*, Technical Report 32-1280. Jet Propulsion Laboratory, Pasadena, Calif., July 15, 1968.
2. Masek, T. D. and Pawlik, E. V., "Thrust System Technology for Solar Electric Propulsion," Paper 68-541, presented at the AIAA Fourth Propulsion Joint Specialist Meeting, Cleveland, Ohio, June 10, 1968.

B. Plasma Investigation in the SE-20C Thruster,

T. D. Masek

1. Introduction

Thruster efficiency improvements in the past 2 yr have resulted from configuration changes (Refs. 1–3). In addition, the influence of operating parameters (propellant flowrate, discharge voltage, magnetic field strength, and ion accelerating voltage) on efficiency has been studied (Refs. 2 and 3). Since thruster efficiency depends directly on the characteristics of the discharge plasma, a study of the plasma in an improved thruster (SE-20C) is of interest. Such a study is required to evaluate the efficiency improvements, determine efficiency limits, and understand the influence of the operating parameters. This article describes the test setup and a portion of the preliminary results of a study with these goals. A conventional Langmuir probe was used to measure plasma properties.

2. Experimental Setup

In order to obtain probe measurements throughout the thruster rapidly, a motor-driven probe positioner was built (Fig. 4). The drive assembly, mounted near the thruster in the chamber, provided radial and axial positioning with positions determined by potentiometers. The potentiometer readings were displayed on an X–Y recorder. A layout of possible probe positions and mechanical interference was used on the recorder to simplify positioning. A set of probe traces, taken on an X–Y–Y recorder, for about 70 positions throughout the thruster, could be obtained in 1 h.

3. Test Results

The plasma properties (electron energy distribution function ion density and plasma potential) of the improved thruster are basically similar to those reported previously (Ref. 4). That is, the electron energy distribution is still composed of primary and maxwellian groups and the density and potentials are of the same order of magnitude as before. The present article will discuss typical data obtained with the improved thruster and give a brief comparison with older thruster data. Analysis of the non-maxwellian characteristics was accomplished as discussed in Ref. 5.

Data taken with a flowrate of 8.8 g/h and 90% utilization efficiency is shown in Figs. 5 and 6. Equivalue curves are estimated in these figures for ion density and plasma potential. Plots for a flowrate of 5.7 g/h and

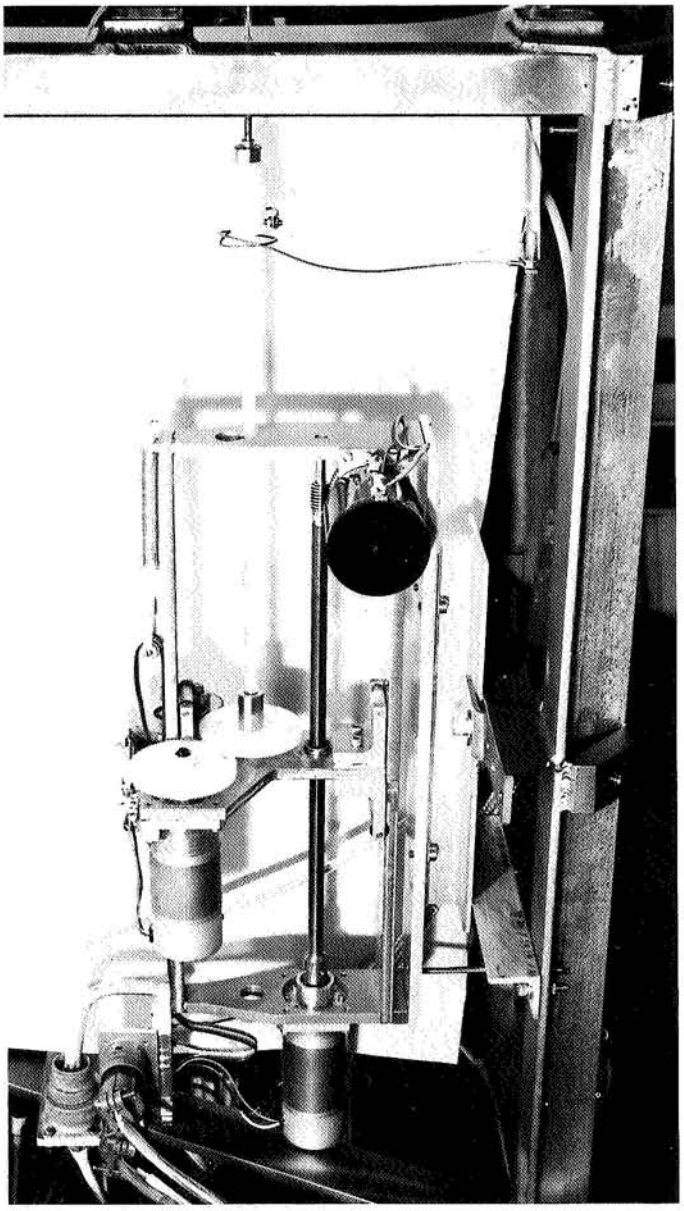

Fig. 4. Probe drive assembly

90% utilization resulted in similarly shaped curves but with somewhat different values. The measured values of each property are indicated at each probe location. Also shown on the figures are the discharge chamber surfaces (cathode, anode screen grid, and housing).

The ion density at the grid (Fig. 5) is seen to vary by only a factor of 3 from the center to 0.9 of the radius. This variation in unimproved thrusters (Ref. 1) was on the order of 10. In addition, the axial variation of density, from maximum to the grid, on the center line is about 2.2, compared with about 1.4 in the older thruster. These differences, in part, result in higher ion axial drift velocity in the plasma and a more uniform ion beam for the improved thruster.

The plasma potential distribution (Fig. 6) plays a principal role in directing ions through the plasma to the grid. The maximum axial variation of potential on the center line is seen to be 2.4 V (compared with less than 1 V maximum in the unimproved thruster). This axial variation at other radial locations is 1.9 V or above. The radial change in potential, from the center line to 0.9 of the radius, varies from 1.4 to 2.0 V over most of the chamber. In addition, about 80% of the locations on the grid side of axial position 4.0 have higher axial potential gradients than radial gradients. This tends to accelerate a large fraction of the ions preferentially toward the grid. The unimproved thruster plasma potential peak was located 0.3 of the chamber length from the grid and had higher radial than axial potential gradient throughout. The density and potential distributions providing higher axial and lower radial ion velocities indicate the manner in which the newer thruster has improved.

The remaining plasma properties also play an important role in thruster operation. However, the differences between these data and those of older thrusters do not appear to contribute greatly to the thruster improvements. The variation of these properties, as well as the potential and density, must be considered in evaluating performance variations with operating conditions. This subject will be discussed in future articles.

References

1. Bechtel, R. T., "Discharge Chamber Optimization of the SERT II Thruster," Paper 67-668, presented at the AIAA Electric Propulsion and Plasmadynamics Conference, Colorado Springs, Colo., Sept. 1967.
2. Masek, T. D. and Pawlik, E. V., "Thrust System Technology for Solar Electric Propulsion," Paper 68-541, presented at the AIAA Fourth Propulsion Joint Specialist Meeting, Cleveland, Ohio, June 10, 1968.
3. Masek, T. D., *Experimental Studies With a Mercury Bombardment Thruster System*, Technical Report 32-1280. Jet Propulsion Laboratory, Pasadena, Calif., July 15, 1968.
4. Masek, T. D., *Plasma Characteristics of the Electron Bombardment Ion Engine*, Technical Report 32-1271. Jet Propulsion Laboratory, Pasadena, Calif., Apr. 15, 1968.
5. Strickfaden, W. B., and Geiler, K. L., "Probe Measurements of the Discharge in an Operating Electron Bombardment Thruster," *AIAA J.*, Vol. I, pp. 1815–1823, 1963.

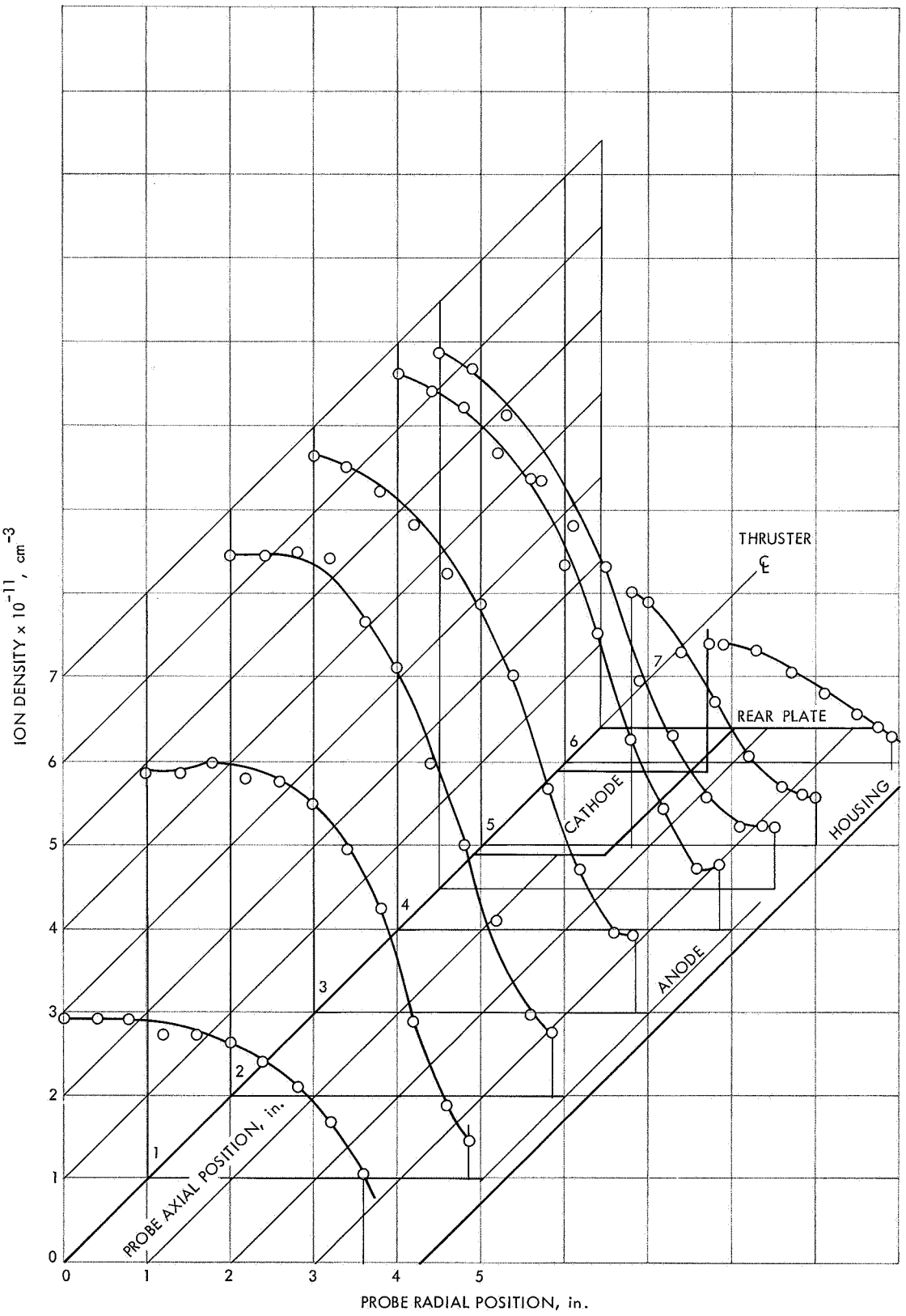

Fig. 5. Ion density distribution in the SE-20C thruster (flowrate = 8.8 g/h, utilization = 90%)

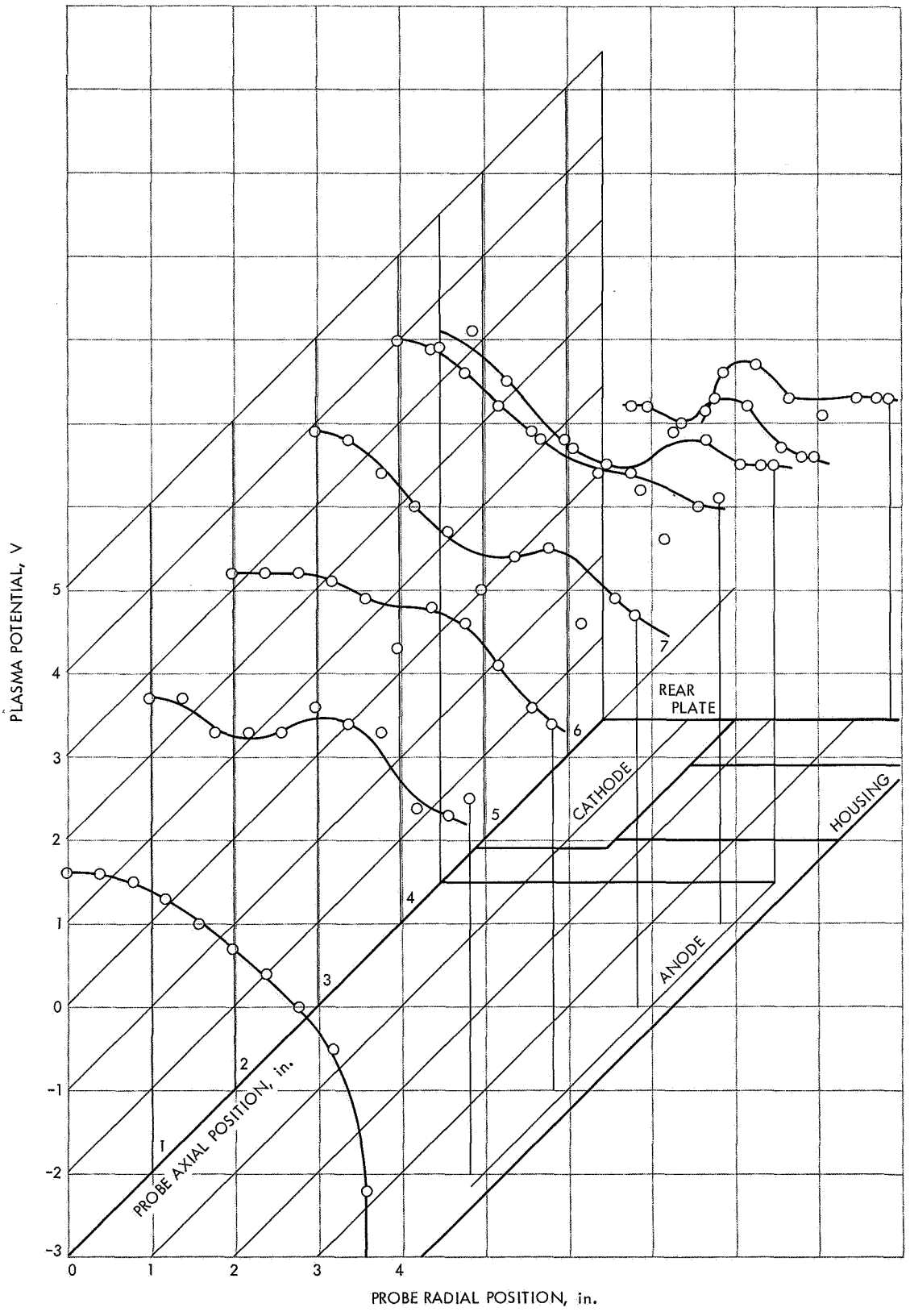

Fig. 6. Plasma potential distribution in the SE-20C thruster (flowrate = 8.8 g/h, utilization = 90%)

C. Liquid–Metal MHD Power Conversion,

D. J. Cerini

1. Introduction

Liquid–metal magnetohydrodynamic (MHD) power conversion is being investigated as a power source for nuclear–electric propulsion. A liquid–metal MHD system has no moving mechanical parts and operates at heat-source temperatures between 1600 and 2000°F. Thus, the system has the potential of high reliability and long lifetime using readily available containment materials such as Nb–1%Zr.

In the particular MHD cycle being investigated, liquid lithium would be (1) heated at about 150 psia in the reactor or reactor-loop heat exchanger; (2) mixed with liquid cesium at the inlet of a two-phase nozzle, causing the cesium to vaporize; (3) accelerated by the cesium to about 500 ft/s at 15 psia; (4) separated from the cesium; (5) decelerated in an alternating-current MHD generator; and (6) returned through a diffuser to the heat source. The cesium would be condensed in a radiator or radiator-loop heat exchanger and returned to the nozzle by an MHD pump.

2. Generator Tests

The ac generator for the NaK–nitrogen conversion system (SPS 37-51, Vol. III, pp. 120–124) is undergoing empty-channel electrical tests. The empty-channel generator tests have the fourfold purpose of (1) providing an operational checkout of the facility instrumentation and electrical control systems; (2) determining the operating characteristics of the generator, with regard to balancing the eight generator phase circuits, in order to obtain a uniform traveling magnetic field with proper upstream and downstream compensating-pole fields; (3) determining the power losses due to induced eddy currents in the structural components of the generator assembly, which includes the laminated stator blocks, the stator clamps (H-frames), stator to H-frame bolts, copper side bars, stator slot plugs (laminated and solid), downstream diffuser, upstream and downstream compensating-pole vanes; and (4) determining the winding loss of the actual coils as a function of traveling-wave magnetic field and frequency.

The generator tested consists of the stator assembly described in SPS 37-50, Vol. III, pp. 182–186, with Litz wire coils as shown in Fig. 7. Shown also is the coolant tank which is raised while testing to immerse the generator in the Freon TF coolant; the gaussmeter probe is used to map the channel magnetic field, and also provides a calibration of the search coils, which are individual wires inserted in each of the stator teeth. By comparison of the voltage induced in any two search-coil wires during NaK–nitrogen system tests, this calibration will permit the evaluation of the magnetic-field amplitude and wave speed in the channel between the two wires.

The search coils and gaussmeter probe were used as an aid in setting the proper phase currents and capacitance values to achieve the desired channel field. A variable capacitor bank on each of the eight generator phases provides the reactive power to the coils, with a five-phase 40-kV-A motor generator set supplying the real power to the two compensating-pole phases and to three of the traveling-wave phases; the remaining three traveling-wave phases are excited by transformer coupling to the three driven phases to produce a six-phase system.

To achieve a balanced operating condition at any current or magnetic field level, the six traveling-wave phase currents are set equal; the compensating-pole currents are set approximately at twice the traveling-wave current; the magnetic field in the upstream and downstream compensating poles is set by rotating the compensating-pole current phase angles to produce maximum downward flux at $\omega t = 0$ and 180 deg, respectively, where $\omega t = 0$ and 90 deg are the times at which the magnetic field has a positive sine wave and negative cosine wave shape, respectively, in the traveling-wave region. Further adjustment of the compensating-pole current amplitudes and phase angle may then be needed to make the search coils at the inlet, center, and exit of the traveling wave equal in phase and magnitude, indicating that the field is symmetrical about the channel midpoint and the flux in both compensating poles is equal to one half the amount of flux in the traveling-wave region. Equal search coil magnitudes and 30-deg phase spacing between adjacent search coils indicate a uniform amplitude and velocity of the traveling wave. Shown in Fig. 8 is a typical magnetic-field survey obtained with the aid of a waveform analyzer which outputs the magnetic-field amplitude at the preset value of ωt to an X–Y plotter.

None of the generator structural components mentioned above had a significant effect on the field shape except for the aluminum downstream diffuser, which fits into generator gap in the downstream compensating pole; this had sufficiently high induced eddy currents and associated magnetic field to completely cancel the desired

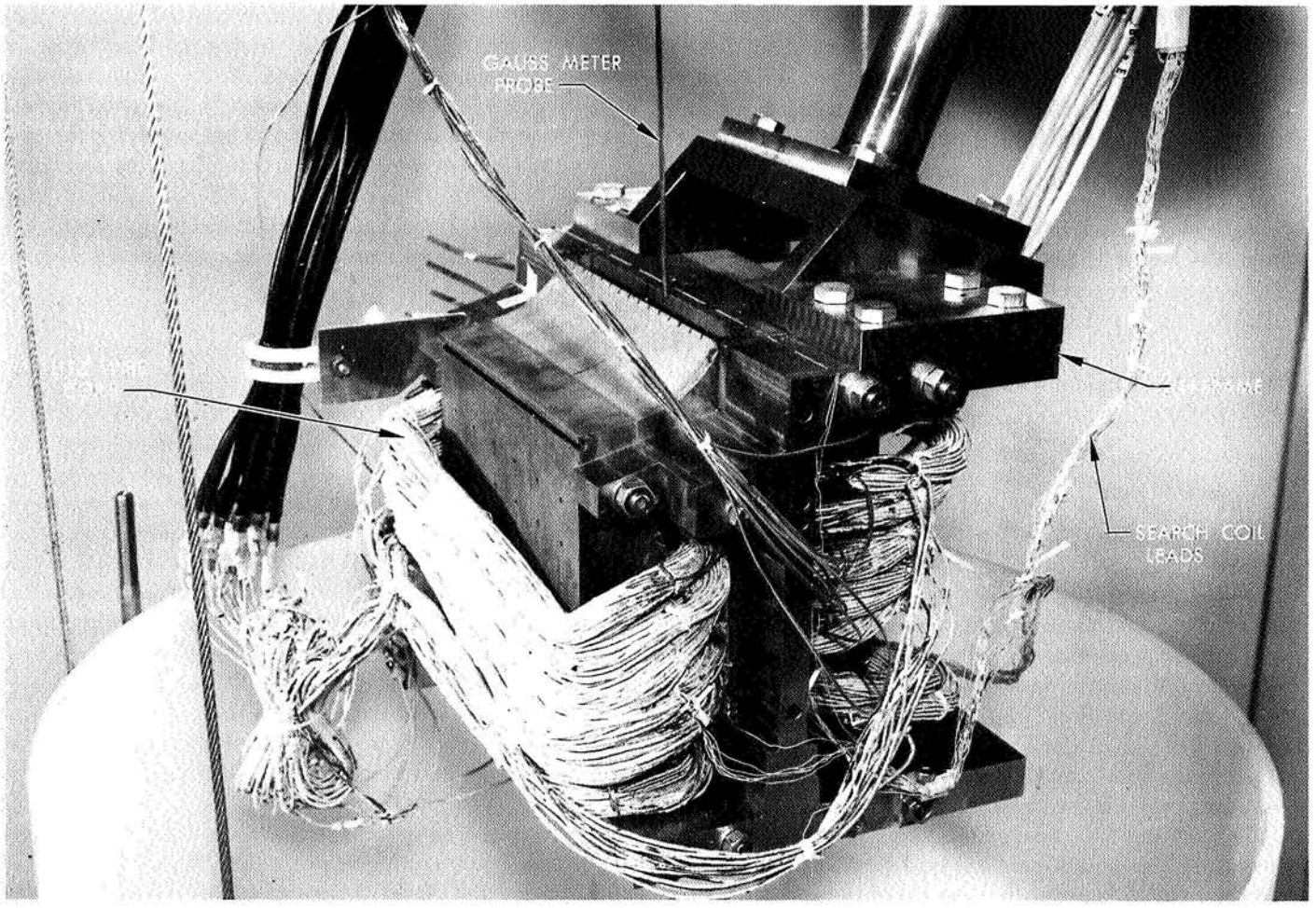

Fig. 7. Test arrangement for measuring generator core losses and magnetic-field profiles

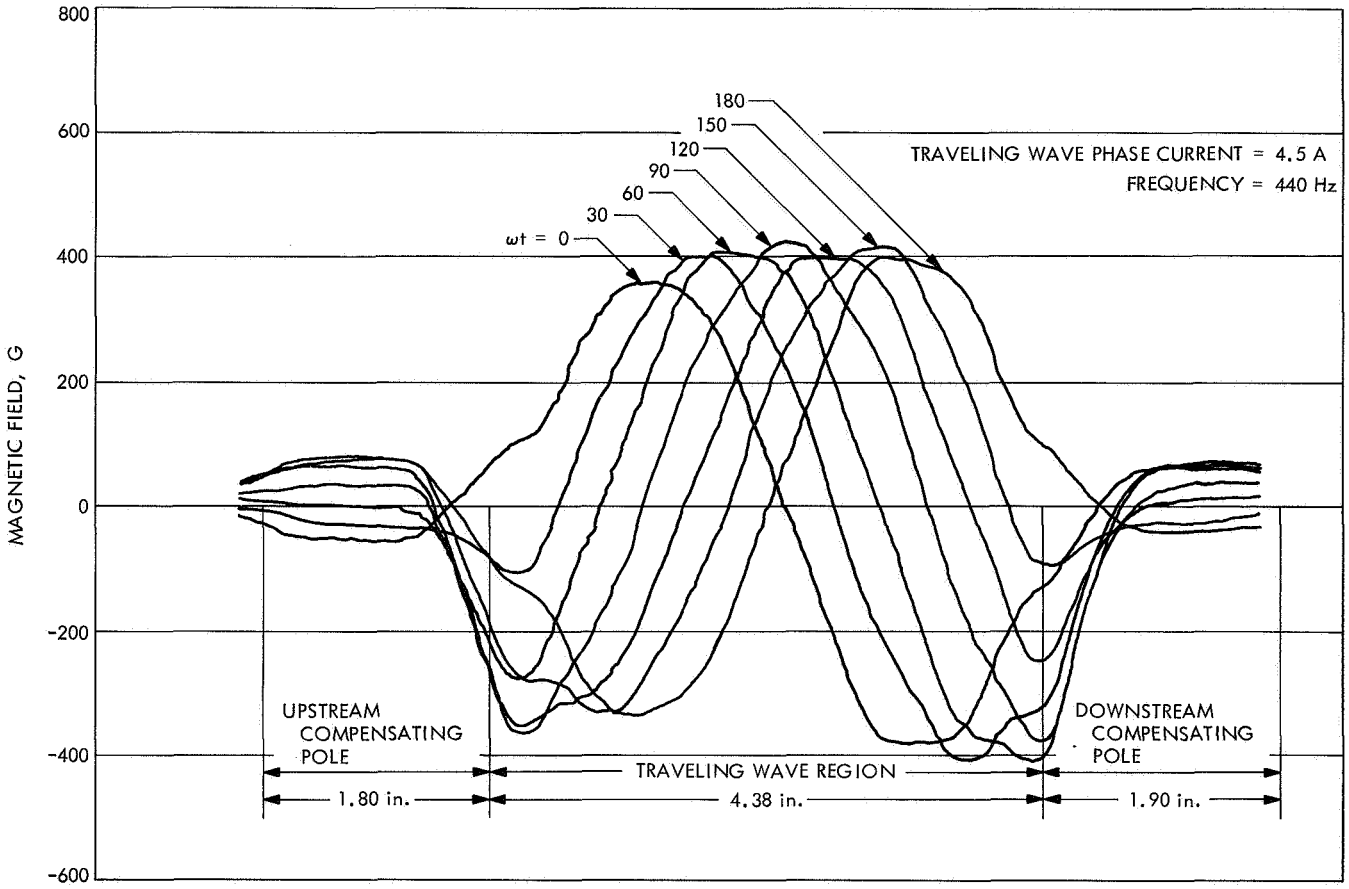

Fig. 8. Measured ac magnetic-field profiles in NaK-nitrogen conversion system generator

compensating-pole field. This result will require the use of a non-metallic diffuser inlet, which was fabricated previously out of Vespel.

Subsequent power-loss tests indicated that other structural components required modification because of excessive power loss even though they had no effect on the field shape. With only the stators and coils assembled, the power loss in the stator blocks due to eddy currents was evaluated as the total input power to the eight phases less the winding power, which is the product of the Litz coil dc resistance and the square of the rms current summed for the eight phases. Extrapolating the power loss to the nominal operating condition indicates an excessive core loss of about 6 kW, which is apparently due to burrs shorting the laminations as evidenced by the low ohmic resistance of the block of about 0.1 Ω.

Subsequent disassembly and acid etch have returned the stator resistance to greater than 6 Ω. The copper side bars, H-frame bolts, and H-frames were added to the stator assembly with a power-loss measurement taken after each was added. The results indicate the copper side bars and bolts will have an acceptable 1-kW power loss, while the H-frames will have an excessive 6-kW loss attributed to their high permeability produced by heat treating. Annealing is expected to reduce the permeability and thus the power loss to an acceptable level without appreciably reducing the mechanical strength. The generator is being reassembled to verify the power-loss reduction in the stators and H-frames and to complete the tests with the addition of the slot plugs and vanes.

D. Potential Distribution Associated With a Glow Discharge Influenced by a Transverse Gas Flow, *J. A. Gardner and M. B. Noel*

1. Introduction

Preliminary experimental investigations concerning flow visualization studies as related to the effects of a transverse gas velocity on a glow discharge were reported

in SPS 37-45, Vol. IV, pp. 162–167. The objective of those initial experiments was to determine in a qualitative sense the influence of a transverse velocity on a glow discharge in the absence of an applied magnetic field.

Additional experiments have now been conducted in which the potential distribution within the electrical discharge region has been obtained by means of a probe. The same parallel-plate copper electrodes that were used previously (Fig. 9) were employed in this investigation. The final objective of these investigations is to achieve a better understanding of the many combinations of processes that occur in the electrical discharge region at and near the electrode surfaces of electrical propulsion and power generation devices.

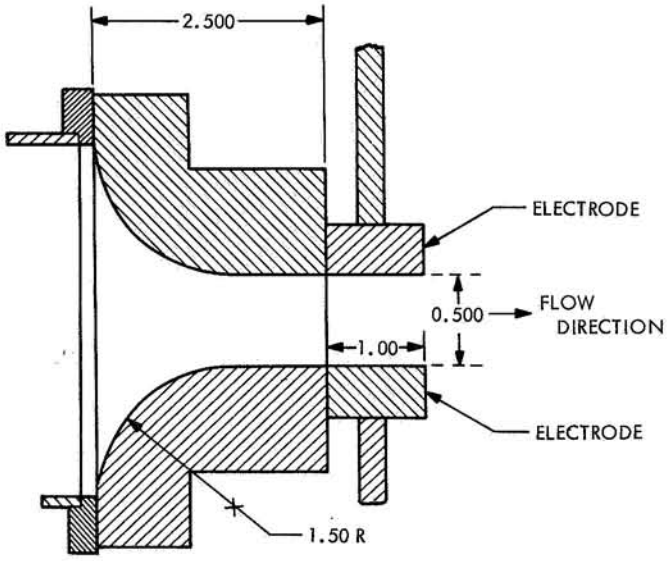

DIMENSIONS IN INCHES

Fig. 9. Experimental apparatus, showing two-dimensional subsonic nozzle and electrode configuration

The effect of blowing on the visual appearance of the discharge was discussed in SPS 37-45, Vol. IV, and is shown in Fig. 10. These photographs indicated that there is most likely a considerable change associated with the electric-field distribution between the static and dynamic conditions. The electric-field distribution for a plasma column between flat parallel-plate electrodes without blowing has been reported by several investigators, e.g., Ref. 1. The anode and cathode fall regions located near the electrode surfaces account for a large fraction of the potential drop. The region between the cathode and

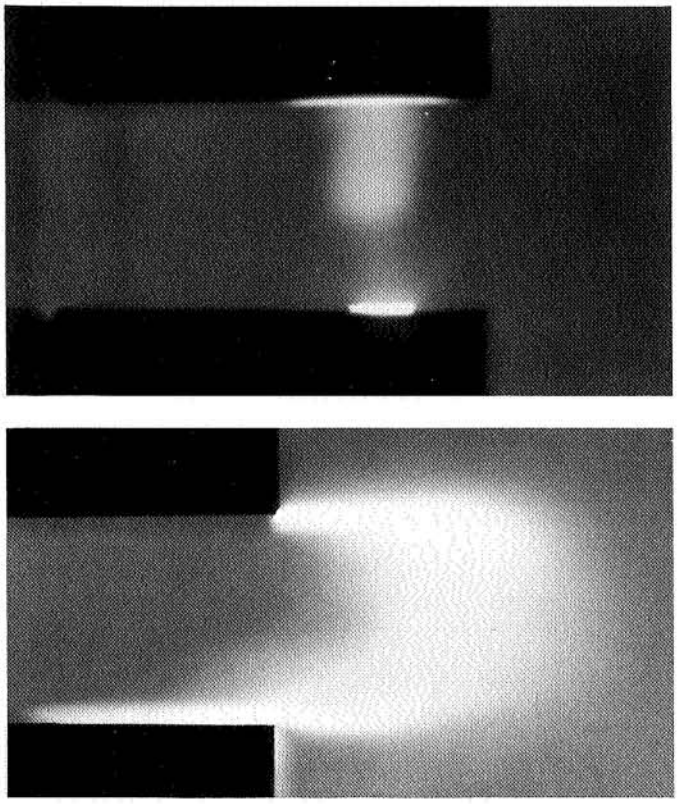

Fig. 10. Glow discharge in argon for a ½-in. electrode separation (15-mA discharge current, 100-torr static pressure): (a) no flow, (b) 127-ft/s flow

anode fall regions is the area where the electric-field gradient is essentially constant. However, in the presence of a transverse gas flow the electric-field distribution becomes quite distorted.

2. Experimental Apparatus

The apparatus used for these experiments (Fig. 9) consisted of a pair of flat parallel copper electrodes enclosed in a six-port glass chamber. Argon gas entered the region between the electrodes at ambient temperature and at a pressure of 100 mm Hg from a two-dimensional convergent nozzle having throat dimensions of 0.5×2.0 in. From the electrode region, the gas flowed into the exhaust duct and the vacuum system. The experiments were conducted at a gas velocity of 127 ft/s, which was computed from the measured total mass flow rate, the pressure and temperature of the gas, and the cross sectional area of the nozzle throat. In prior experiments, pitot tube traverses were performed in the absence of a discharge to verify the uniformity of velocity at the nozzle exit.

3. Procedure and Results

The flow was first established at the desired conditions and then the discharge was initiated and the current level set at 15 mA. Steady state (as determined by visual observation) occurred quickly and remained for an extended period. The local potential was then measured using a 0.010-in.-diam wire enclosed in a needle-shaped glass probe (Fig. 11). The other end of the wire was connected to a 100-MΩ voltmeter and referenced to the cathode (lower electrode in photograph). This electric probe was then traversed in three normal directions to map out the potential distribution.

A portion of this data is presented in Fig. 12. This represents the potential measurement that would correspond to the view seen in the dynamic case (Fig. 10b) taken in the plane of the discharge. The plasma column visually appeared to be approximately 1/16-in. thick in the plane of the photograph and was essentially planar. The shape of the potential curve normal to the velocity vector and normal to the plane of the photograph was symmetrical with respect to the plasma column.

As observed previously, the transverse flow of gas caused the discharge to distort into a U-shape and attach to the trailing edge of the anode. The attachment

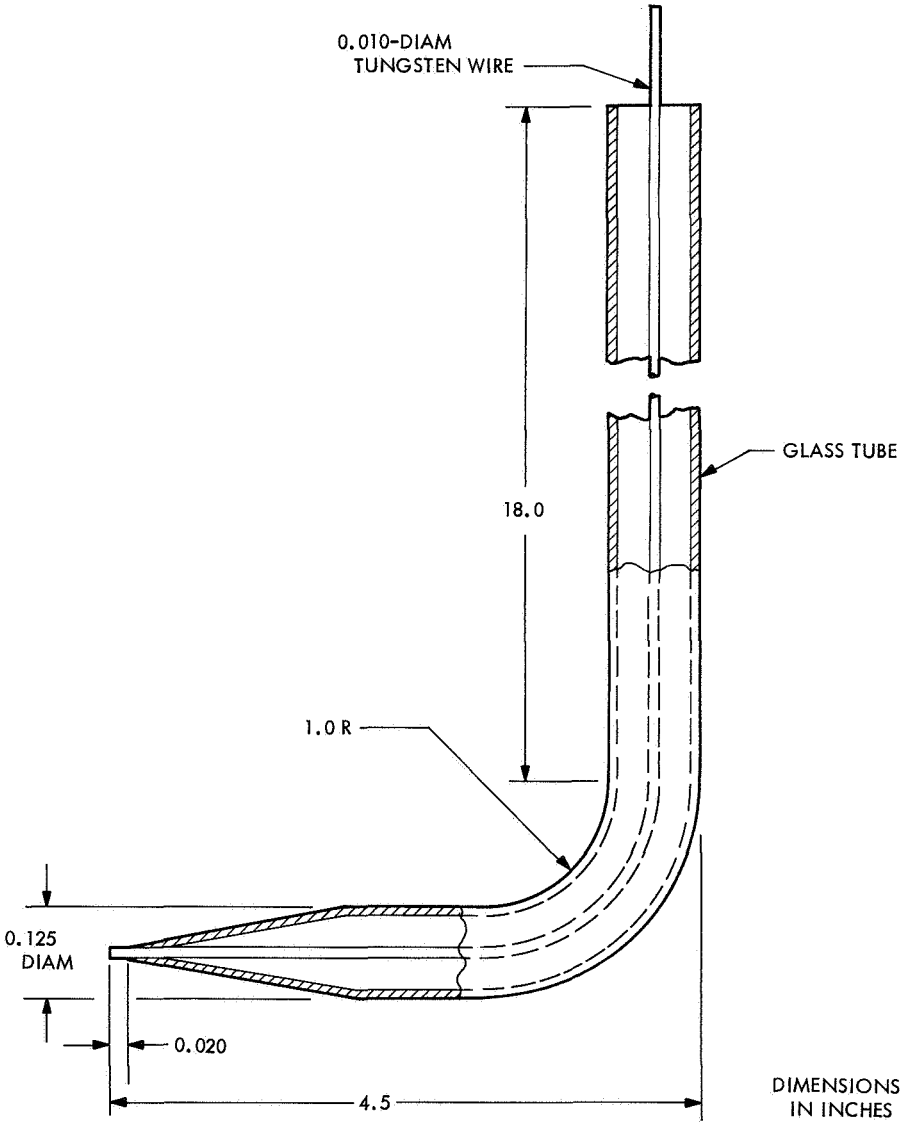

Fig. 11. Glass tube containing tungsten wire

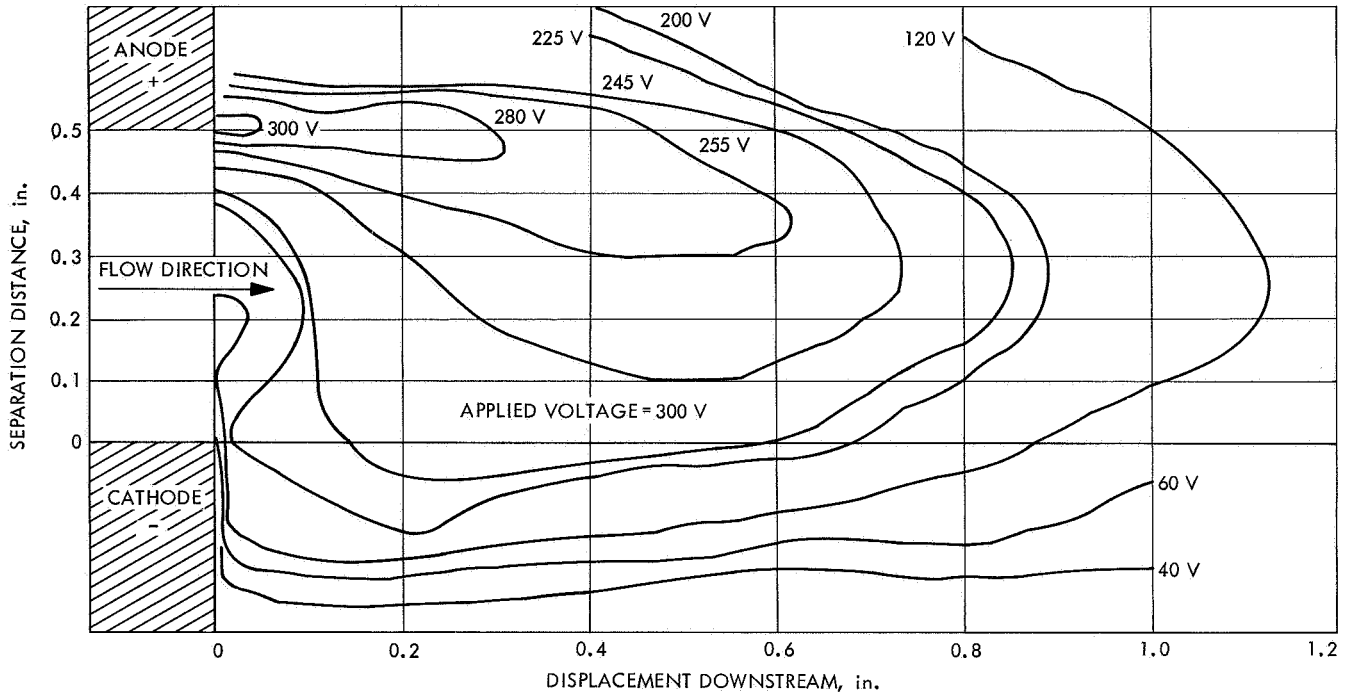

Fig. 12. Potential distribution in plane of plasma discharge affected by 127-ft/s transverse gas flow, 100-torr pressure, and 15-mA current

at the cathode was larger in size than at the anode and extended around the trailing edge. The potential distribution (Fig. 12) in the plane of the discharge is highly distorted in comparison to the static case and appears to correspond with that anticipated from the visual appearance of the plasma column. Constant potential lines shown in Fig. 12 are time-average steady-state values. The applied voltage between the electrodes was 300 V. Assessment of the fall regions cannot be accomplished realistically from Fig. 12, particularly since the data shown is for one plane only. It seems evident, however, that the largest gradient occurred at the trailing edge of the cathode.

4. Conclusions

Severe distortions of the potential distribution, and hence current distribution, caused by a transverse flow field introduce significant complexity into theoretical approaches that might be attempted for computing heat transfer to the electrodes. The flow regions both outside and within the boundary layer of a downstream electrode in a device containing segmented electrodes can be greatly influenced by the effect of blowing on the electrical discharges upstream. For the analysis to be realistic, free-stream conditions at the edge of the boundary layer may require specification of current distributions that are both longitudinal and transverse to the flow direction. Furthermore, these currents may be associated with upstream electrodes.

Reference

1. Thiene, P., "Convective Flexure of a Plasma Conductor," *Phys. Fluids*, Vol. 6, p. 1319, 1963.